TU DELFT

Positron annihilation studies of sodium zirconium phosphate based ceramic materials and Boom clay in the context of radioactive waste isolation and disposal

by

Wietse Hoogsteen

Bachelor Thesis for the bachelor Applied Physics December 2016

Abstract

Generation of nuclear power creates radioactive waste, this waste needs to be stored in a geological repository eventually. Two materials are examined that could be as a potential barrier to contain this waste, sodium zirconium phosphate (NZP, $NaZr_2(PO_4)_3$) based ceramic materials and Boom clay. NZP has a set of positive properties such as chemical and thermal stability and a high isomorphic capability. Because of the high isomorphic capability a wide variety of elements can be inserted into the vacant sites in the host framework. In this thesis phosphates are studied as potential forms for fission product Sr-90.

$$Sr_{1-(x/2)}[Zr_{1+x}Fe_{1-x}(PO_4)_3] \tag{1}$$

were x is varied from 0 to 1 with steps of 0.2. These solid solutions are studied with Doppler Broadening positron Annihilation Radiation (DBAR), in combination with X-Ray Diffraction (XRD).

Clay is an interesting material because of its low permeability, high sorption capacity and plasticity. Boom clay formations in the Netherlands are suitable for geological disposal of nuclear waste. The clay is examined after heating it to determine the relation of the nanoporosity to the water/pyrite concentration. The porosity is closely related to the permeability and therefore related to the capability to contain nuclear waste. This study is done with DBAR, Positron Annihilation Lifetime Spectroscopy (PALS), XRD and Differential Scanning Calorimetry and derivative Thermoravimetry (DSC-TG).

Contents

Chapter 1

Introduction

Radioactive materials are used and generated in medicine, research, education, industry and electricity production. Using radioactive materials creates radioactive waste, this waste needs to be stored such that it forms no health or environmental risks. In the Netherlands COVRA collects, treats and stores the waste. After a storage period of around 100 years the waste is intended for disposal in a geological repository, this means it is stored in deep underground formations. This minimizes the risks to the environment and exposure to future generations. The waste is put into a container consisting of multiple layers of materials to keep radioactive products from leaking out and to stop the radiation from penetrating to the soil[1], this is called the multibarrier system. In 2015 the European Commission invested 3.9 million euros to: "*support the implementation of geological disposal by improving significantly the knowledge base for the Safety Case for European repository concepts.[2]*" In this thesis two types of materials are discussed that can be useful materials to store the radioactive waste in, NZP-phosphates and dutch Boom clay. NZP-phosphates can be useful in the waste form section of the multibarrier system and Boom clay as host rock.

1.1 NZP Phosphates

The current material for the waste form section of the multibarrier system is borosilicate glass, these glasses however have some disadvantages in the form of devitrification, the crystallization of amorphous glass which happens in the presence of water, and also thermodynamic instability as demonstrated by Montel

et al. [3][4]. NZP materials have a good chemical and thermal stability and a very high isomorphic capacity which is a great feature for immobilizing radioactive waste [5][3]. This isomorphic capability is also shown by Subba Rao et al. [6]. Because of this isomorphic capability the molecular structure can be changed such that there are empty positions where radioactive materials can be trapped in. Although ceramics are considered as alternative waste forms, they might be very suitable for the incorporation of separated waste fractions, such as heat-generating Cs-Sr fraction of waste.

Phosphates already showed to have great potential with respect to absorption of radio active waste in Oklo. In 1972 a natural nuclear fission reactor was found near Oklo in Gabon. They found that a lot of the fission products were captured in surrounding phosphates minerals; *Our first surprise was the location of the xenon. It was not, as we had expected, found to a significant extent in the uranium-rich mineral grains. Rather the lions share was trapped in aluminum phosphate minerals, which contain no uranium at all. Remarkably, these grains showed the highest concentration of xenon ever found in any natural material.[7]*

1.2 Boom clay

The Boom clay is studied as potential host rock in the multibarrier system for geological disposal of radioactive waste in the Netherlands and Belgium because of the isolating potential of low permeable, clay-rich rocks [8]. High-level waste emits significant amounts of heat for hundreds or thousands of years. This thermal load can affect the properties of clay with respect to nuclear waste disposal such as permeability, porosity and solubility. It is shown by Jie Han et al.[9] that the porosity of clay increases with temperature. In 2013 a large scale heating test was done by Ph. Van Marcke et al. [10] where they investigated the impact of a large-scale thermal load on the Boom clay. In this thesis small scale experiments will be done at higher temperatures to investigate the changes in porosity with temperature.

1.3 Goal

In this research we will be focusing on molecular vacancies and defects. Radioactive materials can be trapped in these vacancies which can affect the isolation properties with respect to radioactive waste. It has been shown that positrons are a powerfull tool to explore the adsorption, pore filling, porosity and surface properties of various systems[11]. In the study done by Eric R et al. [12] it is shown nanoporosity (0.5 nm) is detectable by positrons in Metakaolin-based geopolymers. P Guagliardo et al. [13] showed that molecular vacancies in pollucite can be measured with the help of positron studies. K. Leluka et al. [14] discovered that changes in interlayer distances between lattices in kaolinite can be 'seen' by positrons. So the vacancies, porosity and defects of Boom clay and NZP Phosphates will be studied with the help of positrons. The technique used is Doppler Broadening Annihilation Radiation (DBAR) and Positron Lifetime Annihilation Radiation (PALS).

Chapter 2

Materials and Methods

2.1 NZP Phosphates

The material studied in this experiment is the sodium zirconium phosphate (NZP) structural family, of which $NaZr_2(PO_4)_3$ is the parent composition. The NZP structure was first determined by Hagman[15]. They found that NZP crystallizes in a trigonal crystal system, with lattice hexagonal and space group $R\bar{3}c$. NZP type ceramics are based on the natural minerals kosnarite (2.1), the simplest NZP is also its synthetic analogue: sodium zirconium phosphate (2.2). The crystal chemical formula for the NZP type structure is 2.3, here M1 and M2 are void cations that fill the cavities in the framework, whilst L cations fill the framework. In the case of sodium zirconium phosphate only the M1 cavities are filled. [3]

$$K[Zr_2(PO_4)_3] \tag{2.1}$$

$$Na[Zr_2(PO_4)_3] \tag{2.2}$$

$$(M1)(M2)_3[L_2(PO_4)_3] \tag{2.3}$$

As briefly mentioned in the introduction NZP materials have good chemical and thermal stability and an exceptional quality of these materials is its isomorphic capacity which allows to include up to two thirds of the elements of the Periodic table in its composition which is a great feature for immobilizing radioactive waste.[5]

In this research we will be looking into these materials with positrons mainly. To see if positron measurements can give us insight to the vacancies in these structures where fission products can be captured. Radioactive materials can be trapped in these vacancies which can affect the isolation properties with respect to radioactive waste.

In this thesis we inserted Strontium in the molecular structure, to mimic the incorporation of radioactive fission product Sr-90.

$$Sr_{1-(x/2)}[Zr_{1+x}Fe_{1-x}(PO_4)_3] \tag{1}$$

Six samples were made with different vacancy densities. This is done by inserting atoms with different valencies in the positions of the structure. The atoms are strontium (2), zirconium(4) and iron(3) in this case. When more zirconium and less strontium is introduced, less positions need to be filled to achieve neutral charge in the molecule. The two end members of this formula are plotted with Vesta[16]. The structural data of the solutions $Sr[ZrFe(PO_4)_3]$[17] and $Sr_{1/2}[Zr_2(PO_4)_3]$[18] were found in the Pearson Crystal Database [19]. It is shown in figures 2.1 and 2.2 that the solution with $x = 1$ has more vacant sites in the molecular structure.

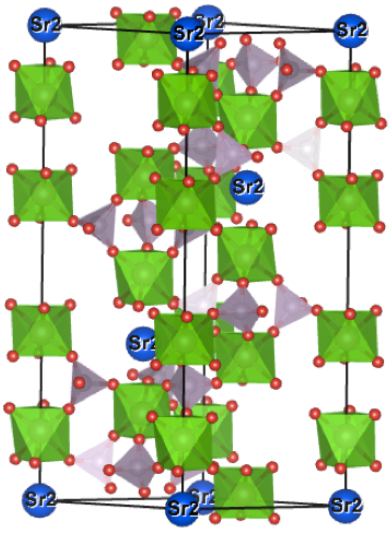

FIGURE 2.1: Structure model of $Sr_{1/2}[Zr_2(PO_4)_3]$ made using Vesta software with data from the Pearson Crystal Database. The blue spheres represent the strontium atoms, the red dots the oxygen atoms. ($x = 1$, High vacancy density)

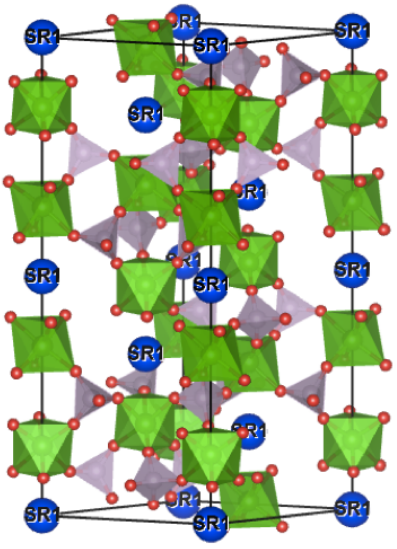

FIGURE 2.2: Structure model of $Sr[ZrFe(PO_4)_3]$ ($x = 0$ Low vacancy density)

2.2 Boom clay

The favourable properties of clay formations in general for disposal of radioactive waste include[20]:

- Low permeability and low hydraulic gradients
- Chemical buffering capacity
- Propensity for plastic deformation and self-sealing of fractures
- Geochemical characteristics that favour low solubility of radionuclides
- High capacity to retard the migration of radionuclides towards the accessible environment, e.g. through sorption capacity and due to a diffusion-dominated transport

The distribution and depth of the Boom clay formations in the Netherlands were investigated in CORA[21]. These formations are named in the Netherlands as Rupel formations[22]. The age of these formations range from 30 to 34 million years (the epoch Oligocene [23] in the Cenozoic era).[24]

The Boom clay is selected as potential host rock for geological disposal of radioactive waste in the Netherlands because of the isolating potential of low permeable, clay-rich rocks.[25]. The low permeability results in very slow water movements in

FIGURE 2.3: Boom clay in quary near Leuven [8]

the host rock, and a good ability to retain radionuclides by physico-chemical adsorption on clay minerals. [26] The clay is also very accessible in the Netherlands as can be seen in figure 2.4.

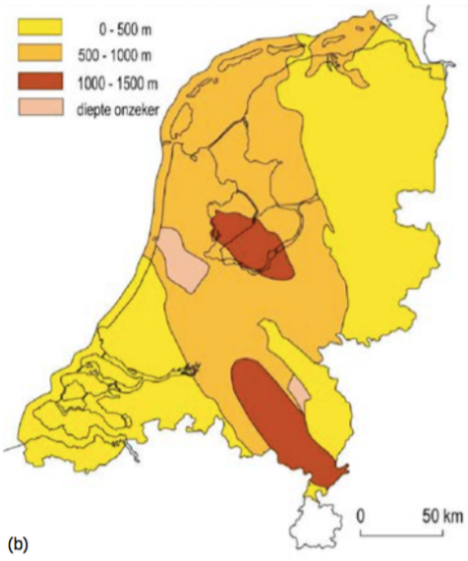

FIGURE 2.4: Depth map of available Boom clay in the Netherlands[27]

The boom clay seen in figure 2.3 comes from Leuven in Belgium, the sample available at the RID comes from Zeeland in the Netherlands. The sample is taken at a depth of 80 meters. X-ray diffraction was done on the Boom clay. As you can see in figure 2.5 the main phases are quartz (SiO_2), pyrite (FeS_2) and Muscovite ($KAl_2(AlSi_3)O_{10})(F, OH)_2$).

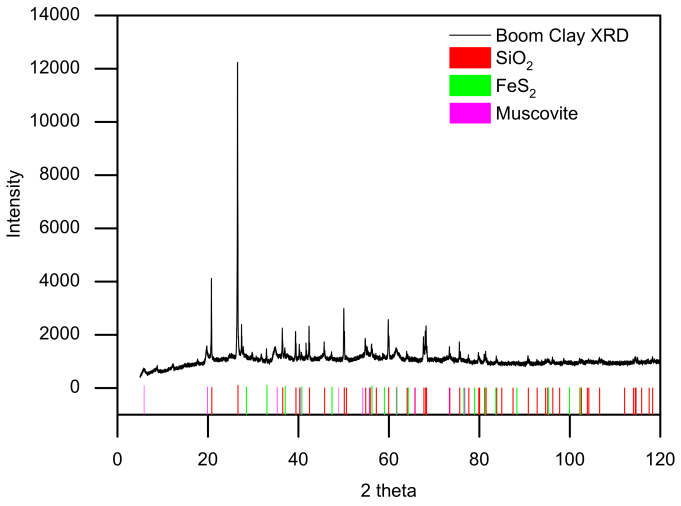

FIGURE 2.5: XRD of Dutch Boom clay with quartz, pyrite and muscovite the three main phases. [28]

To investigate the Boom clay, we heat it to see what happens to the clay-minerals and water content. For example, water evaporates and the pyrite oxidizes. This can increase porosity which can affect the permeability and transport properties of radionuclides in the clay. This is especially relevant in the case of heat generating radioactive waste.

2.3 Positron Source

The source used in both experiments is ^{22}Na which decays in the following way.

$$^{22}Na \rightarrow ^{22} Ne + \beta^{+} + v_e + \gamma \tag{2.4}$$

^{22}Na has a very high positron yield of 90.4% as can be seen from figure 2.6[29]. It has several other advantages such as the appearance of a 1.27 MeV γ almost simultaneous with the positron. This allows lifetime measurements to be conducted with a start-stop γ detector. Sodium salts are also easy to handle and the price is reasonable, this makes it the most widely used positron source.

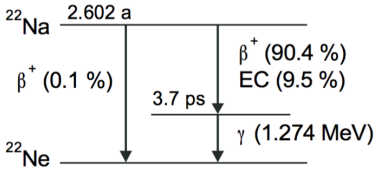

FIGURE 2.6: Decay scheme of ^{22}Na, 90.4% decays by emission of a positron and an electron neutrino to the excited state of ^{22}Ne. [29]

2.4 Positron Doppler Broadening Annihilation Radiation (DBAR)

If positrons are inserted in solid state materials, information is obtained by studying the characteristics of the gamma rays arising from the annihilation of a positron and an electron.

$$e^+ + e^- = 2\gamma \tag{2.5}$$

Conservation of energy and momentum requires that if the electron (or positron) has a non-zero momentum, the energies of the gamma's are given by equations 2.6 and 2.7. If the annihilation pair has a nonzero momentum, the two gamma rays have an angle deviating from π as shown in figure 2.7. The angles are given by 2.8 and 2.9.

$$E_\gamma = m_e c^2 \pm \Delta E \tag{2.6}$$

$$\Delta E = \frac{p_\parallel c}{2} \tag{2.7}$$

$$\theta_{\gamma\gamma} = \pi - \Delta\theta \tag{2.8}$$

$$\Delta\theta = \frac{p_\perp}{m_e c} \tag{2.9}$$

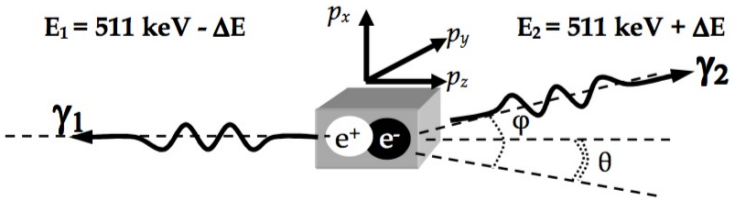

FIGURE 2.7: Schematic representation of the positron-electron annihilation [30]

In Doppler broadening experiments the energy shift of the emitted annihilation photons is measured. This shift is due to the Doppler effect caused by the momentum distribution of the electrons.

The DB study relies on the non-zero component of the momentum of the electrons parallel to the gamma emission (2.7). This results in a shift of the energy of the annihilation photons of a few keVs around 511 keV. This can be detected by the detectors. The results are characterized by the S-parameter (shape) and the W-parameter (wing).

To describe the annihilation spectrum, we use the S-parameter, this parameter is defined as the ratio of the area of central part of the annihilation peak (V) and the total area, see figure 2.8. The absolute value carries no direct physical information but can be a useful parameter to check if there are defects present in a sample. Open volume defects in solid state materials form an attractive potential well for positrons, in these wells the electron density and the electron momentum distribution are different. When a positron encounters a defect it is more likely to annihilate with a low momentum electron. This is because electrons far away from the nucleus have a lower momentum so in defects there are more low momentum electrons. This results in a narrowing of the annihilation peak around 511 keV. The W-parameter, the area C left and right of 511 keV divided by the total area, indicates the fraction of positrons that annihilate with high momentum electrons and is related to the chemical environment where the annihilation takes place.[30]

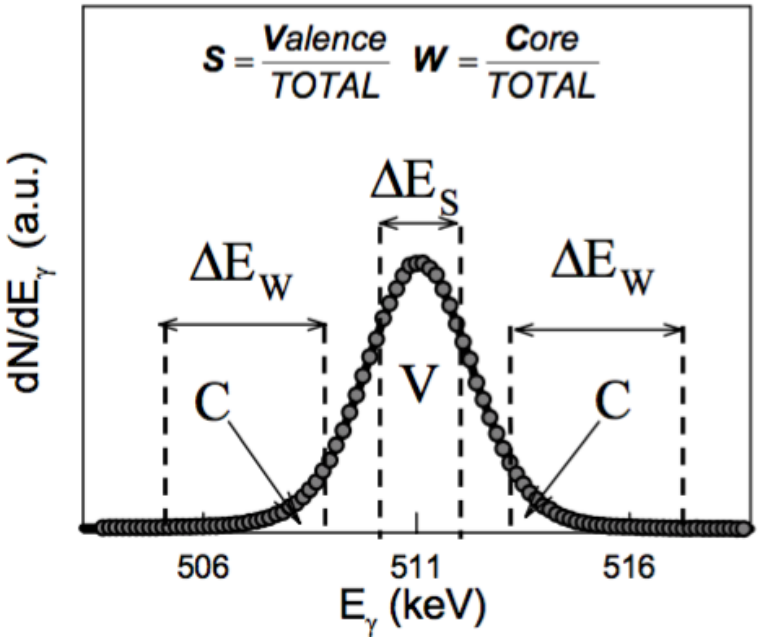

FIGURE 2.8: Definition of Shape and Wing parameter. The surface of V in the range ΔE_s devided by the total surface is the value of the S paramenter[30]

2.5 Positron Annihilation Lifetime Spectroscopy (PALS)

Positron Annihilation Lifetime (PALS) experiments are probably the most widely used positron technique due to its simple experimental setup and direct results. PALS measures the time difference between the emission of a positron and its annihilation with an electron in the sample. When the 1274 keV photon is measured that is emitted simultaneously with the positron, the time measurement starts. When the 511 keV of the positron-electron annihilation is measured, the time measurement stops. When positrons are trapped in open-volume defects, such as vacancies and their agglomerates, the positron lifetime increases with respect to the defect-free sample. This is due to the locally reduced electron density of the defect. Thus, a longer lifetime component, which is a measure of the size of the open volume, appears. The strength of this component, i.e. its intensity, is directly related to the defect concentration. In principle, both items of information, i.e. the kind and concentration of the defect under investigation, can be obtained independently by a single measurement. This is the major advantage of positron lifetime spectroscopy compared with angular correlation of annihilation radiation or Doppler-broadening spectroscopy with respect to defect issues[29]. The theoretical lifetime spectrum is:

$$F(t) = \sum_{i=1}^{N} \frac{I_i}{\tau_i} e^{\frac{-t}{\tau_i}} \tag{2.10}$$

With N the number of positron annihilation components, τ the lifetime and I the intensity of each site. Lifetime spectra are analysed with LT [31]. Typical values for the lifetimes are 100-200 ps for materials without defects/vacancies and 400-500 ps for materials with vacancies.

In some low density materials a positron can capture an electron and form a bound state Positronium (Ps). Positronium exists in two states, para positronium (p-Ps) and ortho positronium (o-Ps). The p-Ps is the singlet state with antiparralel spins and o-Ps is the triplet state with parallel spins. p-Ps decays via 2γ emission and has a lifetime of around 125 ps in vacuum, because o-Ps decays via 3γ emission it has a much longer lifetime of 142 ns. [32][33][34] In matter the lifetime of o-Ps is significantly shorter due to a so called 'pick-off' process in which a positron of

o-Ps annihilates with an electron of the material with opposite spin and then via 2γ decay. Materials with open volumes that allow the formation of Ps the lifetime reaches 1-2 ns. [30]

In figure 2.9 below a PALS measurement is shown with the corresponding lifetimes.

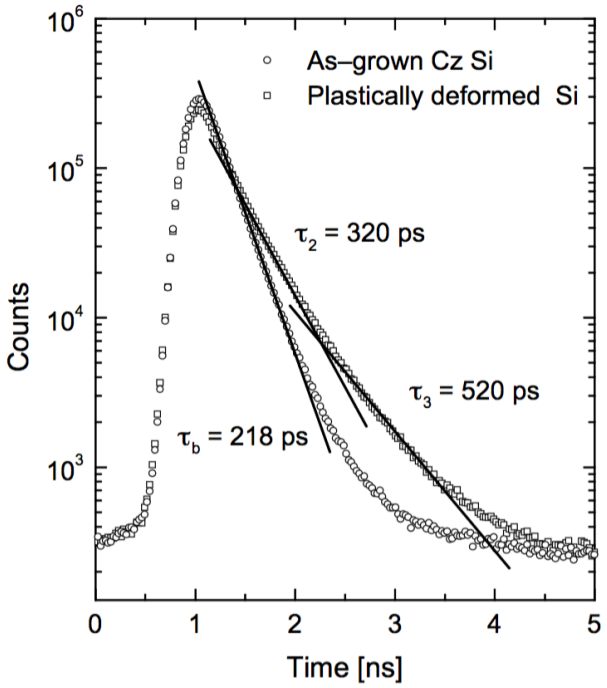

FIGURE 2.9: Positron lifetime spectra of as-grown and Czochralski-grown (Cz) silicon (Hubner et al. 1997b). The curve of Czochralski-grown is located higher which indicates longer lifetimes and thus a higher defect concentration [29]

The curve on the left hand side is related to the resolution of the measurement.

2.6 X-ray diffraction (XRD)

X-ray diffraction (XRD) is a technique used for phase identification of a the crystalline material and can provides information on unit cell dimensions. Because the wavelength of X-ray's is similar to the spacing of lattice planes in atomic structures, these lattice planes act as diffraction gratings for X-rays. This technique is based on constructive interference of monochromatic X-rays in a crystalline sample. Constructive inteference occurs when Bragg's Law is satified.[35]

$$n \cdot \lambda = 2d \cdot sin(\theta) \tag{2.11}$$

where n is a positive integer, λ the wavelength of the incomming x-rays, d the distance between lattices and θ the angle between incomming and diffracted rays indicated in figure 2.10. Braggs law relates the wave length of the electromagnetic radiation to the diffraction angle and the lattice spacing within the crystal. The

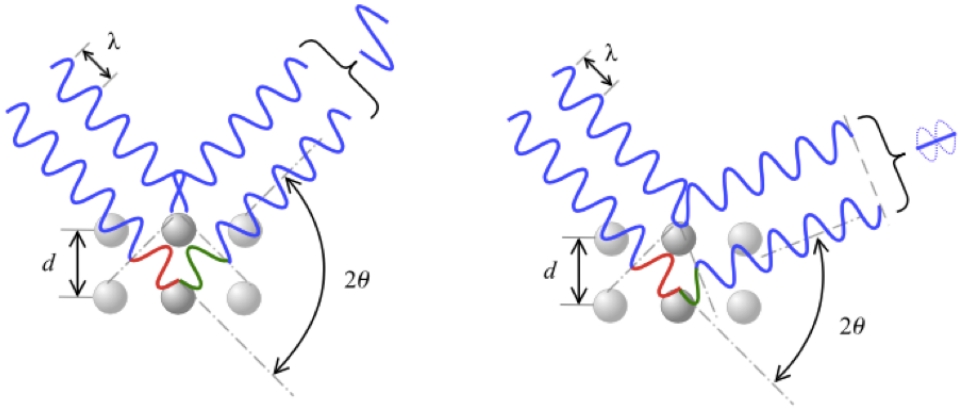

FIGURE 2.10: X-ray diffraction on lattice planes. The angle θ is related to the distance between the lattice planes and the wavelength by Bragg's law [36]

diffracted X-rays are detected and counted. Due to the fact that the orientation of the powdered material is random the detection is done through a range of values of θ. The analyzed material is finely ground, homogenized, and average bulk composition is determined.

2.7 Differential scanning calorimetry and Derivative Thermogravimetry (DSC-TG)

The formal definition of TG according to the Nomenclature Committee of the ICTAC [37] is:'a technique in which the mass of a substance is measured as a function of temperature whilst the substance is subjected to a controlled temperature program'. A thermobalance is used to aqcuire the thermogravimetric curve. The data is then presented with the rate of change in mass with respect to temperature. Mass losses (in percentages) are plotted downward on the vertical axis and the temperature or time on the horizontal axis.[38]

DSC is a method in which the material under investigation is subjected to a programmed temperature change and thermal effects in the material is observed. The

term "differential" indicates that the difference in behavior between the material under investigation and an inert reference material is studied. In this manner the temperature at which any event either absorbs or releases heat can be found. This allows the determination of temperatures at which phase transitions and chemical reactions occur. The record is the differential thermal curve, the temperature difference is plotted on the vertical axis with endothermic processes downward. The temperature is plotted on the horizontal axis.[38]

The advantage of obtaining data in the same sample for both TG and DSC is obvious, you can measure the same sample at the same time. When two thermal analysis systems are investigated separately, the samples can behave differently. A further advantage of using simultaneous techniques concerns the environment around the sample, this is the same when measuring simultaneous.[38]

Chapter 3

Experimental procedure

3.1 Sample Preparation

3.1.1 NZP Phosphates

The samples were synthesised with the use of mechanochemical synthesis. This is shown in figure 3.1. This method relies on ball milling as a means of homogeniza-

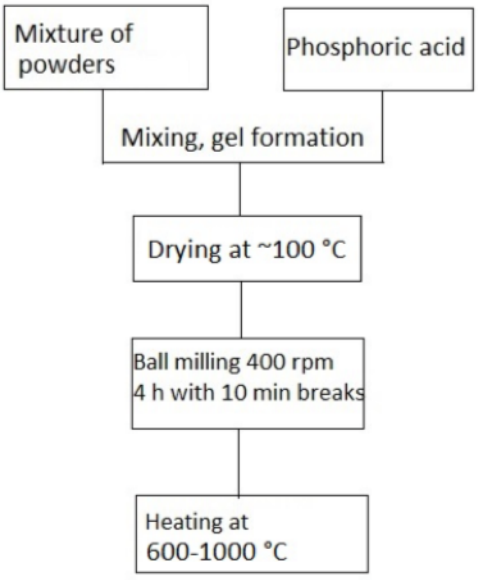

FIGURE 3.1: Mechanochemical synthesis of NZP phosphates [3]

tion and synthesizing an amorphous product. After the milling the powders were subjected to a heat treatment with temperatures ranging from 600°C to 1000°C.[3]

To install the solid solutions in the VEP setup, they had to be made into pellets with a diameter larger than 10 mm. This was done by pressing the powder with a press applying 10 tons of pressure for 2 minutes. The crystallization of the NZP phase starts at around 800°C so the pellets were given a temperature treatment at 600°C for 72 hours, 800°C for 24 hours and 1000°C for 4 hours.

The samples are installed in a metal frame with two wires in the middle. The samples, 1 cm in diameter, 1.0-1.5 mm thick, are then installed between the wires as can be seen in figure 3.2.

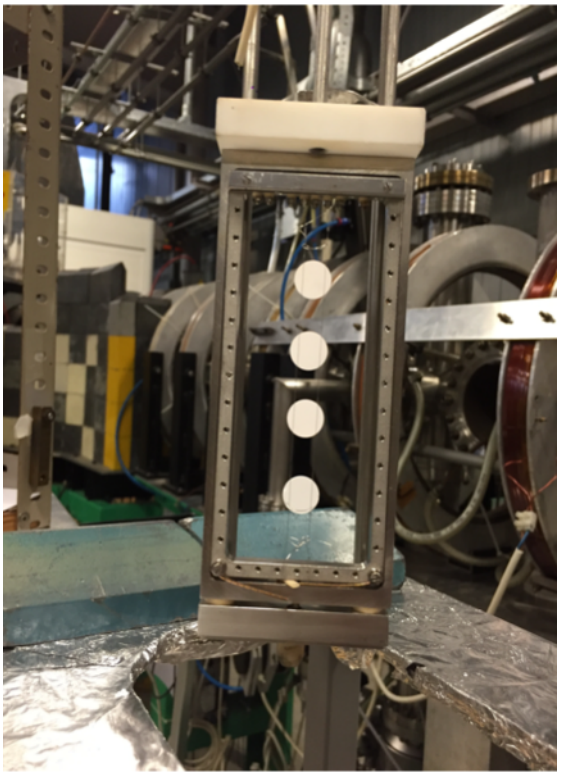

FIGURE 3.2: 4 samples inside metal frame before inserting the frame into the Variable Energy Positron beam (VEP).

3.1.2 Boom clay

The Boom clay sample needed to be prepared in an environment without oxygen to avoid oxidation so it was done inside a glove box filled with nitrogen. A rough piece was broken off and it is sanded down to the desired measurements, roughly one centimeter in diameter and a thickness of 1-2 mm. This sample is then installed in the sample holder (figure 3.3) which goes into the oven.

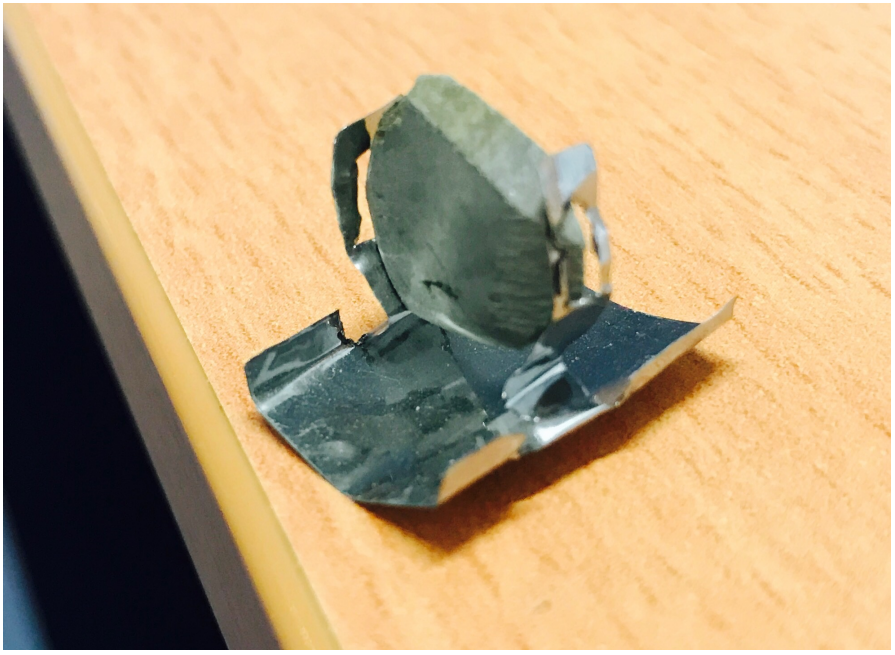

FIGURE 3.3: Boom clay sample in sample holder, this can be inserted into the small oven inside the VEP.

For the temperature measurement of the Boom clay a small oven is installed in the VEP. This is a cylindrical tube with a heating coil around it. The sample is first heated to a set temperature and then cooled down to room temperature. In figure 3.4 the glowing sample is shown inside the oven in the VEP.

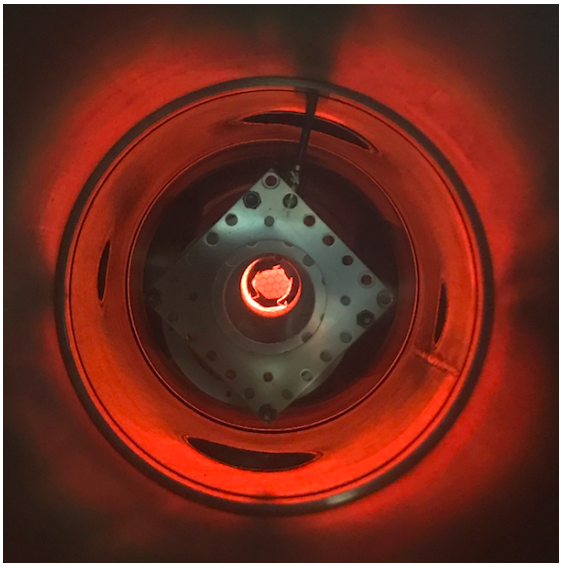

FIGURE 3.4: Heating Boom clay inside VEP at 750°C.

3.2 Experimental setup

3.2.1 Variable Energy Positron beam (VEP)

In this experiment we have used the VEP (variable energy positron beam) positron beam available at the RID in Delft. The VEP beam utilizes ^{22}Na as positron source, with a present activity of about 1 GBq. In DB (Doppler Broadening) mode the implantation energy can be varied between 0.1 and 30 keV with a beam diameter on the target of about 8 mm. The facility is equipped with two Ge detectors for 1D or 2D Doppler Broadening studies.

This isotope emits positrons with a continuous energy spectrum, so moderation is required. In order to obtain depth profiling information, to study thin layers for example, mono-energetic slow positron beams are required. The fast positrons can be slowed down using a moderation step. This is done with moderators with a negative positron work function which re-emits positrons with a much smaller energy spread. After moderation the positron beams energy can be varied by accelerating up the positrons. Because the energy is now variable, depth profiling can be obtained.

To give an idea about what the implantation energy means it is possible to obtain the depth profile P(E,z).

$$P(E,z) = \frac{mz^{m-1}}{z_0^m} e^{-(\frac{z}{z_0})^m} \tag{3.1}$$

$$z_0 = \frac{AE^r}{\rho\Gamma(1+\frac{1}{m})} \tag{3.2}$$

This is called the Makhov profile [39]. Where E is the energy of the mono energetic positrons. And m, r and A are empirical parameters. ρ is the mass density and Γ is the gamma function. These empirical parameters are not determined for the materials used in this study therefore widely used values are inserted; A = 40 $\mu g cm^{-2} keV^{-r}$, $m = 2$ and $r = 1.6$ [40].

$$\bar{z} = \frac{AE^r}{\rho} \tag{3.3}$$

is the mean penetration depth which will be sufficient for this study.

3.2.2 Positron Lifetime Annihilation Spectroscopy (PALS)

The ^{22}Na source is located between two films of kapton and is 'sandwiched' between two clay samples (figure 3.5) so that the samples that need to be measured can be pressed against the source without the risk of contaminating the sample. The first measurement is done with the 'fresh' clay and the second with the clay from the temperature measurement of the VEP. The second sample was heated in the VEP up untill 750°C. The schematic setup and setup used is shown in figure

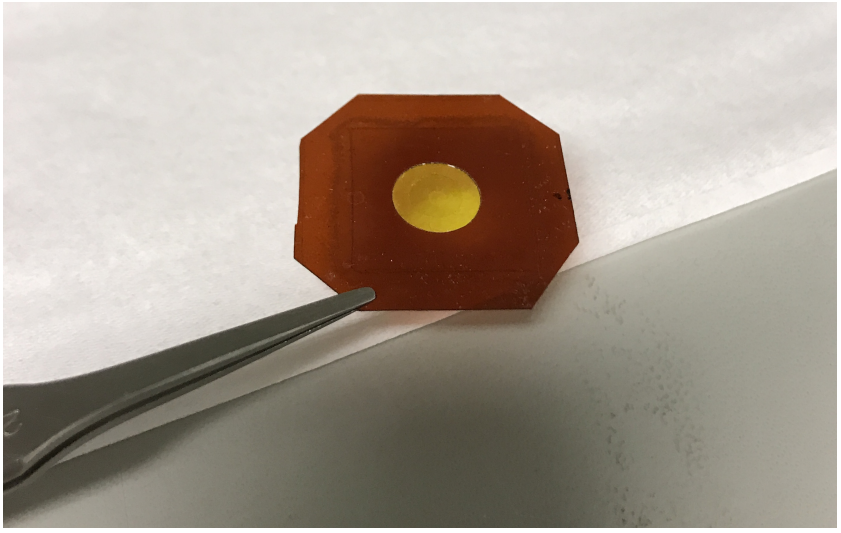

FIGURE 3.5: ^{22}Na source between two thin films of kapton (yellow). The clay samples are put on the top and the bottom of these films.

3.6 and 3.7. There are two photon detectors on either side of the positron source. One detector is wired to the 'start' of a timer and the second to the 'stop'.

3.2.3 XRD and DSC-TG

The X-ray diffraction measurments were done using the instrument X'pert Pro MPD DY2988 from Panalytical. The measurement was done at 45kV, 40mA and angles ranging from 5 - 120 2θ

For the DSC-TG measurment the 96 LINE TGA-DSC [41] was used. A sample of the Boom clay was supplied by COVRA. From this sample a 49,8 mg was taken and installed in the device. The sample was measured up until 1100°C.

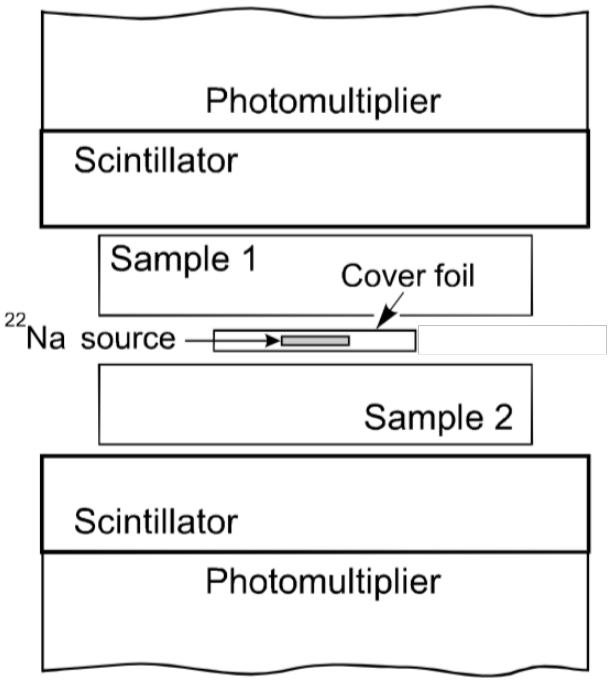

FIGURE 3.6: Schematic representation of the two samples and the positron source 'sandwiched' in between. Sample 1 and 2 represent the Boom clay in this case and the cover foil is kapton.[29]

FIGURE 3.7: PALS setup, the two photon detectors on either side rigged to the 'stopwatch'.

Chapter 4

Results and Discussion

4.1 NZP-Phosphates

4.1.1 DBAR

Figure 4.1 shows the plot of the S-parameter, the plot is made with the use of VEPFIT[42], which uses an algorithm that simulates the implantation and solves the diffusion equation, taking the trapping and annihilation of the positrons into account.

In the plot the S-parameter of the sample with x = 1.0 is higher than that of the sample with x = 0.0 which indicates the positrons in the sample x = 1 annihilate with lower momentum electrons. The density of low momentum electrons is high in open volume defects so we can conclude that sample with x = 1.0 has a higher vacancy density than sample with x = 0.0.

Another useful plot is the SW diagram, this plots the S-parameter value versus the W-parameter. With this it is possible to map a third variable, in this case the value of x. Logically there is a correlation between S and W, but if the plot is linear we can conclude that there are no significant changes to the chemical compositions of the materials. Plotted are the averages of the S and W parameter for each value of x, the averages are taken from a mean implantation depth of 0.1 nm such that surface effects are not taken into account. In figure 4.2 it is shown they lie on a straight line.

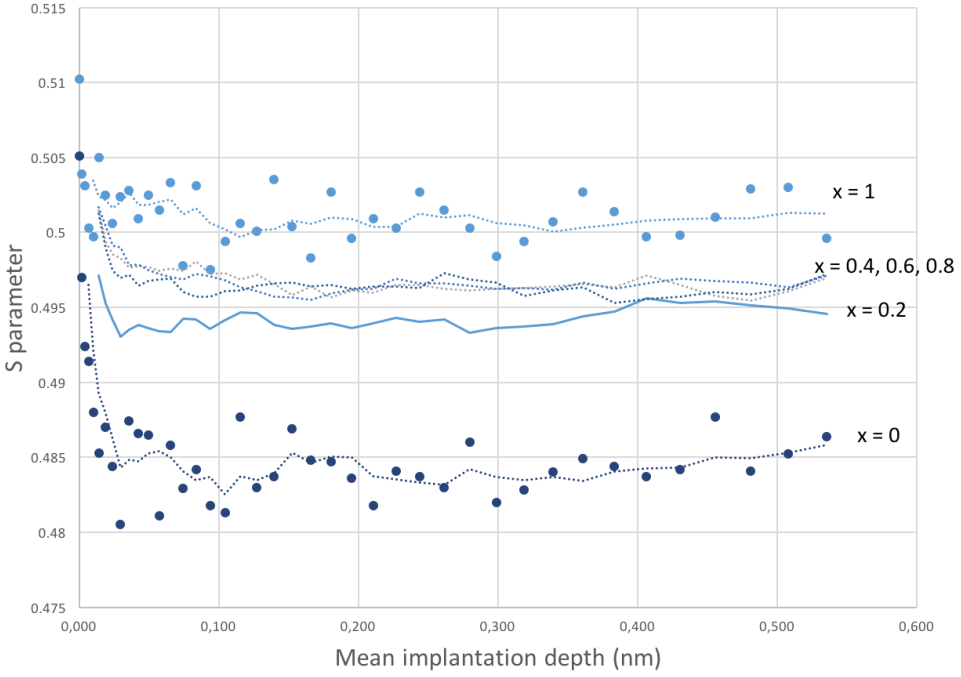

FIGURE 4.1: S-parameter for samples$Sr_{1-(x/2)}[Zr_{1+x}Fe_{1-x}(PO_4)_3]$ with x = 0, 0.2, 0.4, 0.6, 0.8, 1.On the x axis the mean implantation depth from formula 2.9 is plotted, on the y axis the S parameter is plotted. Data points are shown for x = 1 and x = 0.

If we state that in x = 1 all the positrons annihilate in vacancies and all positrons in x = 0 annihilate in the bulk then at x = 0.2 57% of positrons annihilate with low momentum electrons in vacancies. And 72% for the values x = 0.4, 0.6 and 0.8 annihilate in vacancies. This shows most vacancies are created between x = 0 and x = 0.4.

4.1.2 XRD

To determine the chemical composition and the size of the vacancies we used x-ray diffraction to estimate the size of the unit cell. The two end members are know compounds, the data of these are found in Pearson's Crystal Database[19]. The x = 0 sample has the spacegroup $R\bar{3}$ (148)[17] and the x = 1 has spacegroup $R\bar{3}c$ (167)[18]. So this changes when x varies between 0 and 1.

The diffractograms were analyzed with the program Fullprof[43], the program is used as a profile matching or pattern decomposition tool using the Le Bail[44] method. For the samples x = 1, 0.8 and 0.6 the spacegroup 148 is used and for

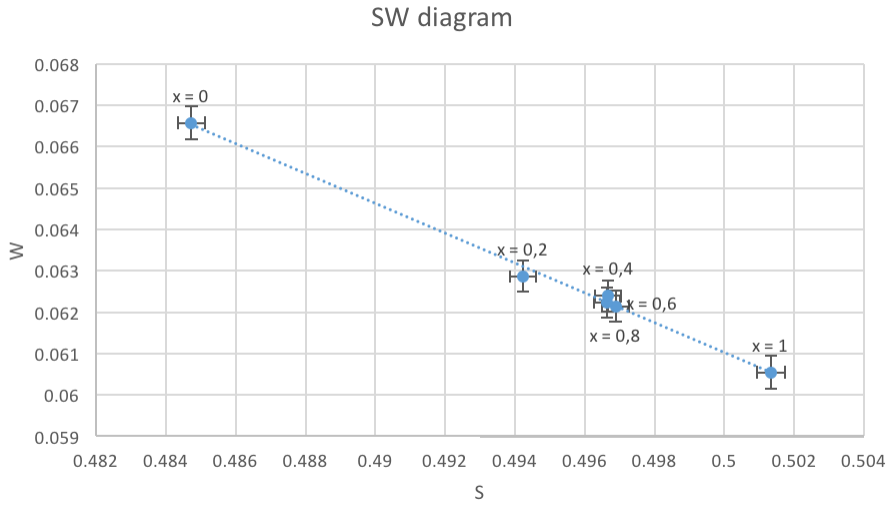

FIGURE 4.2: SW diagram for samples x = 0, 0.2, 0.4, 0.6, 0.8, 1.

the other three the refinement is done with spacegroup 167. The diffractograms of the different compounds of $Sr_{1/2}[Zr_2(PO_4)_3]$ are shown in figure 4.3. All diffrac-

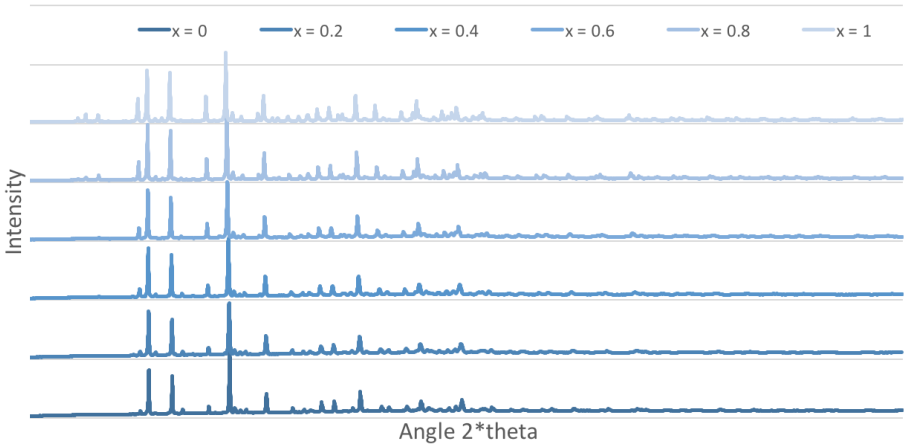

FIGURE 4.3: Diffractograms of the six samples with $x = 0$ on the bottom and $x = 1$ on the top.

tograms look similar, there are a couple of differences though. The three reflections at small angles are visible for x = 1 and x = 0.8 and dissapears for lower values of x. The le Bail refinement of the x = 0.6 compound is shown in figure 4.4, the fit is good enough for calculation of the unit cell parameters.

To calculate the atomic positions Rietveld refinement had to be done with a structural model. The best result obtained was from $Sr_{1/2}[Zr_2(PO_4)_3]$ and is shown below in figure 4.5. The chi-squared values and R-factors of the refinement were not good enough to draw any conclusions from. Possible causes of the inaccuracy

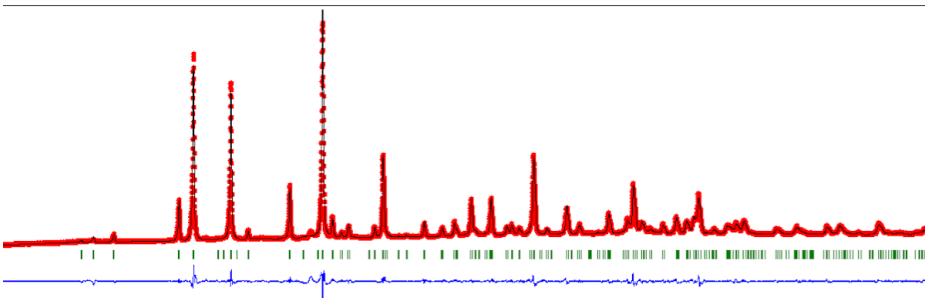

FIGURE 4.4: Le Bail refinement on compound $Sr_{0.7}[Zr_{1.6}(PO_4)_3]$. The red line represents the X-ray diffractogram and the black line shows the Le Bail refinement. The blue line is the difference curve of those two. The chi-squared value is 5.45 and the R-factors are 2.55 and 3.62.

of the refinement are addmixtures and multiple phases inside the sample. This inaccuracy was also a reason to examine the samples with positrons. In figure 4.6 the results of the Le Bail refinement are shown.

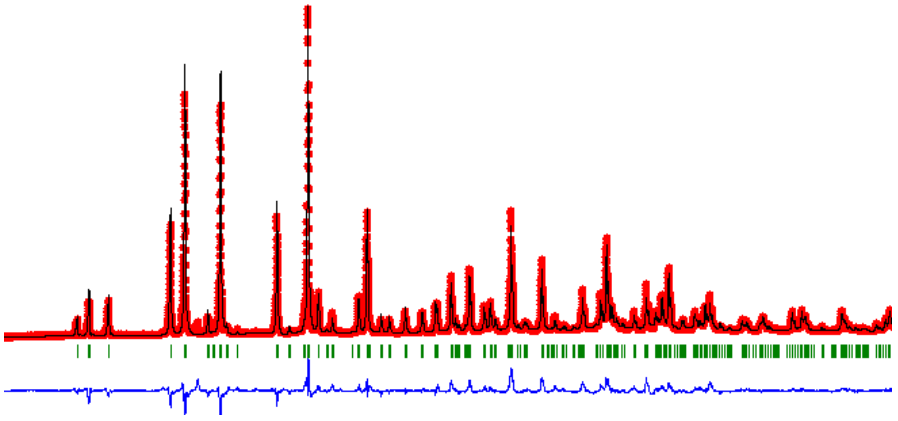

FIGURE 4.5: Rietveld structural refinement of $Sr_{1/2}[Zr_2(PO_4)_3]$. The best chi-squared value obtained is 20.9, not good enough to estimate atomic positions.

Figure 4.6 shows the unit cell volume vs the value of x. The vacancy density is higher in x = 1, from the downward slope it is concluded that the unit cell decreases when the vacancy density decreases.

4.1.3 Discussion

Now it is important to check if the positron data is affected by the vacancies created or just the increasing size of the unit cell, which increases the distance between atoms. To do this the volume of the unit cell is plotted next to the S-parameter in figure 4.7.

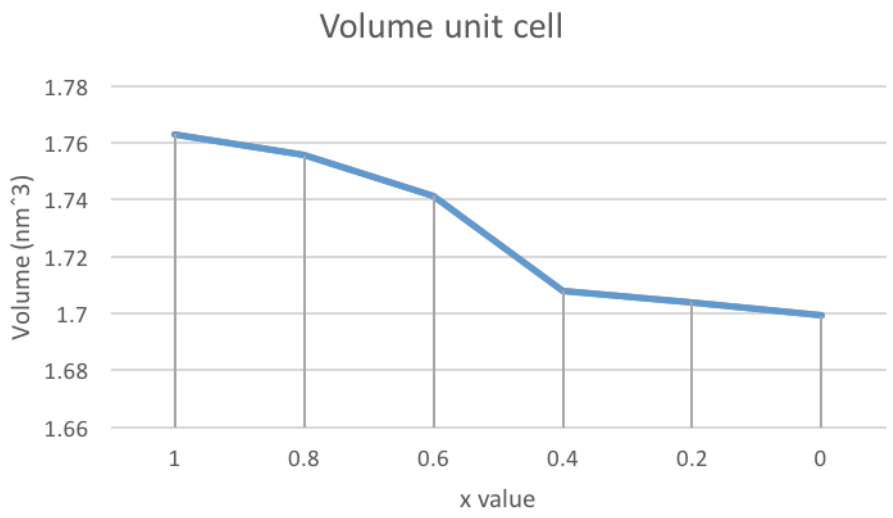

FIGURE 4.6: Unit cell volume, result of the Le Bail refinement.

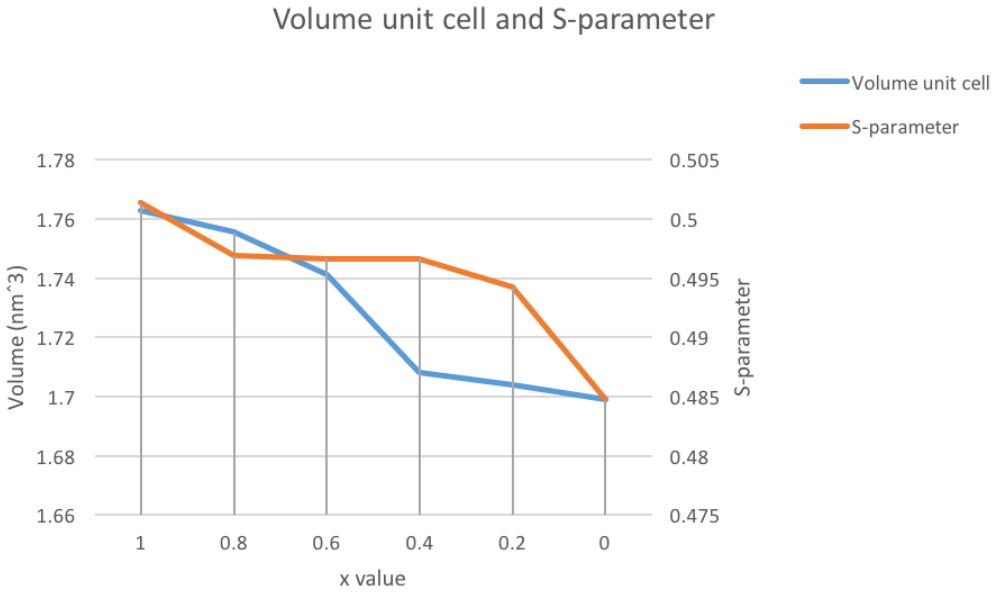

FIGURE 4.7: Volume unit cell and S-parameter sample x = 0 to x = 1. Result of Le Bail refinement and DBAR

So the drop from 0.6 to 0.4 is not seen by the positrons, this drop can be explained by the difference in space group. The S-parameter has two significant drops, from x =1 to x = 0.8 and between x = 0.4 and x = 0. The volume of the unit cell does not decrease a lot in these ranges so it can be concluded the drop in S-parameter is caused by the decreasing vacancy density. Another conclusion we can draw from this result is that from x = 0 to x = 0.2 most of the vacancies have been created

in the molecular structure. If the atomic positions could be determined via the structural refinement of the diffractograms, the sizes of the vacancies could be compared to the value of the S parameter. Unfortunately the precision needed for this was not achieved. Possible reasons are multiple phases and/or add mixtures in the powder.

4.2 Boom clay

4.2.1 DSC-TG

First DSC-TG testing was done on the clay to measure at which temperatures mass loss occurs and endothermic or exothermic processes take place. The results are seen in figure 4.13.

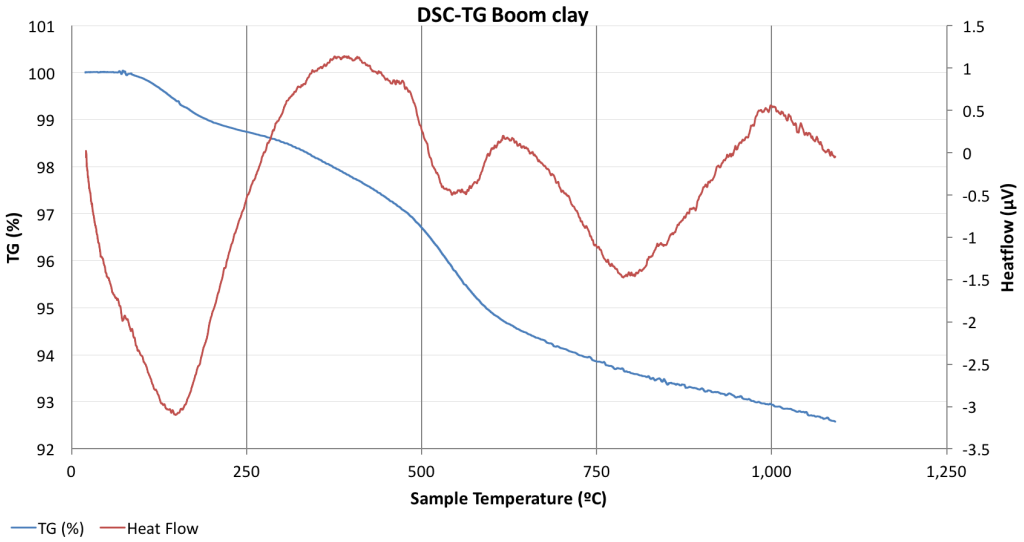

FIGURE 4.8: DSC-TG of Boom clay. The blue curve represents the mass loss in percentages and the red curve represents the heatflow in the sample.

The TG curve first shows the loss of interstitial water at 80-140°C,the second drop between 300°C and 600°C is due to several reactions. From 300-500°C mass loss mainly consists of organics combustion and dissipation of structural water [9][45]. The bigger drop from 500-650°C is the oxidizing of pyrite[46]. The gradual decline at temperatures higher than 650°C the mass loss can be explained by decomposition of the carbonates [46] and dissipation of structural water.

There are three distinct local minima in the DSC curve (red). This means an endothermic process occurs at these temperatures. The first endothermic process from 20-150°C is assigned to the evaporation of water, the second can be explained by the pyrite in the clay oxidizing. The third endothermic process can be explained by decomposition of the carbonates. The last drop at 1000°C can be caused by the $\alpha - \beta$ transition of quartz in the clay, this transition occurs without mass loss[47].

4.2.2 DBAR

In figure 4.9 you can see the S-parameter plotted against the temperature the clay was heated to. A higher S-parameter could indicate a higher concentration of vacancies, defects or open volumes.

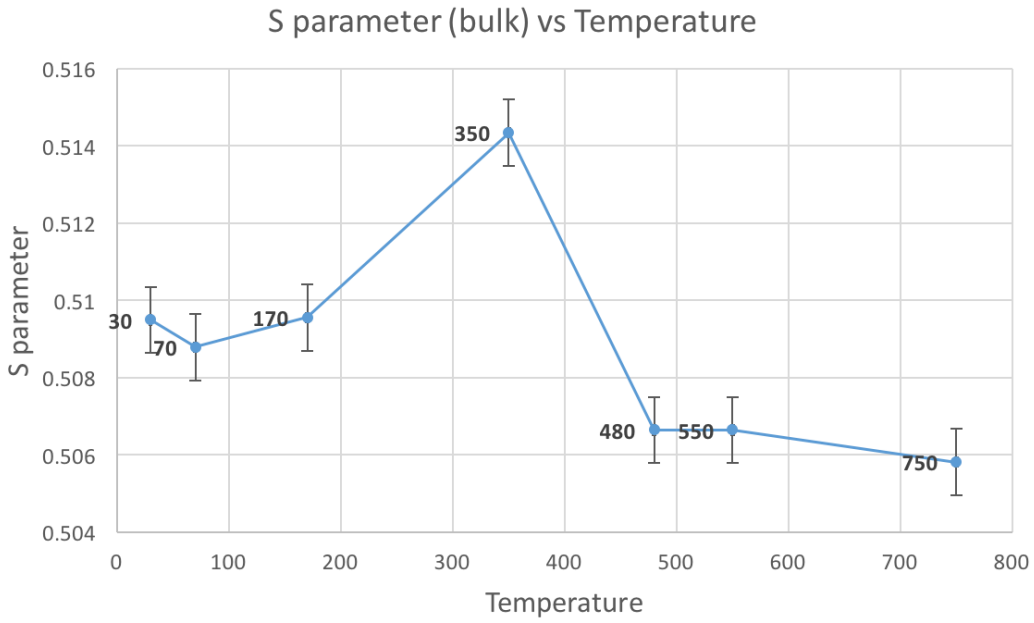

FIGURE 4.9: S-parameter vs temperature, result of the temperature measurement in the VEP

The expectation was that the S-parameter would increase with temperature, this expectation was met up untill 350°C. At 480°C the S-parameter drops to a value below that of the lower temperatures. This indicates some sort of phase transition in the clay when heated above 350°C. To check what caused this effect PALS and XRD measurements were done.

TABLE 4.1: Results of the lifetime measurement on the 'fresh' and heated clay .

	$\tau_1(ns)$	$I_1(\%)$	$\tau_2(ns)$	$I_2(\%)$	$\tau_3(ns)$	$I_3(\%)$
'Fresh' Boom clay	0,193	55,88	0,431	44,12	-	-
Heated Boom clay	0,177	44,42	0,427	54,98	13,5	0,596

4.2.3 PALS

The result of the lifetime measurement of the 'fresh' Boom clay is shown in figure 4.10. It can be seen two lifetime's are present and two contributions of the source. The blue and black curves represent $\tau_1 = 0.193ns$ and $\tau_2 = 0.431ns$ respectively. The slope of the left part of the graph is related to the accuracy of the measurement, in our case this is about 1 nano second. In table 4.1 the results of the PALS measurements are shown. Two samples are measured, the 'fresh' clay and the heated sample from the Doppler Broadening experiment.

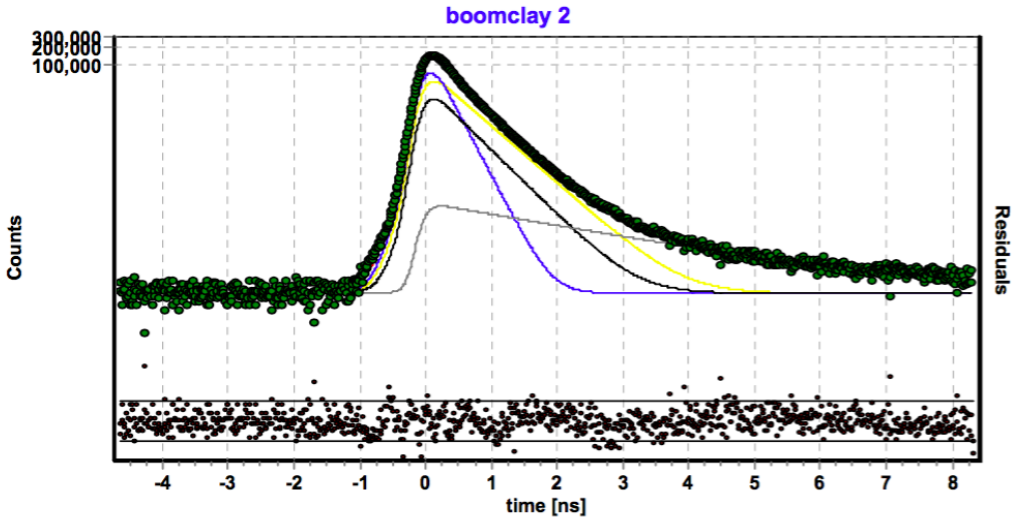

FIGURE 4.10: PALS measurement on the fresh Boom clay. On the y-axis the counts are plotted on a logaritmic scale, the x-axis represents the lifetime in nano seconds. Below the graph the difference plot is shown. The blue and black curves represent $\tau_1 = 0.193ns$ and $\tau_2 = 0.431ns$ respectively.

The heated clay shows a third lifetime component, this is a very long lifetime that can only be explained by the formation of positronium. This indicates larger open volumes in the heated clay. The heated sample has a somewhat shorter lifetime at both τ_1 and τ_2 which is in line with the Doppler Broadening experiment. However I_2 is significantly higher for the heated sample.

4.2.4 XRD

XRD was done on the heated clay sample. With the program HighScore [48] the diffractogram can be analyzed and the main phases can be found via a database search and match tool. It is shown in figure 4.11 the main phases are quartz (SiO_2), corundum Al_2O_3 and muscovite ($KAl_2(AlSi_3)O_{10})(F,OH)_2$). The main difference with the fresh clay is the absence of pyrite and the appearance of corundum.

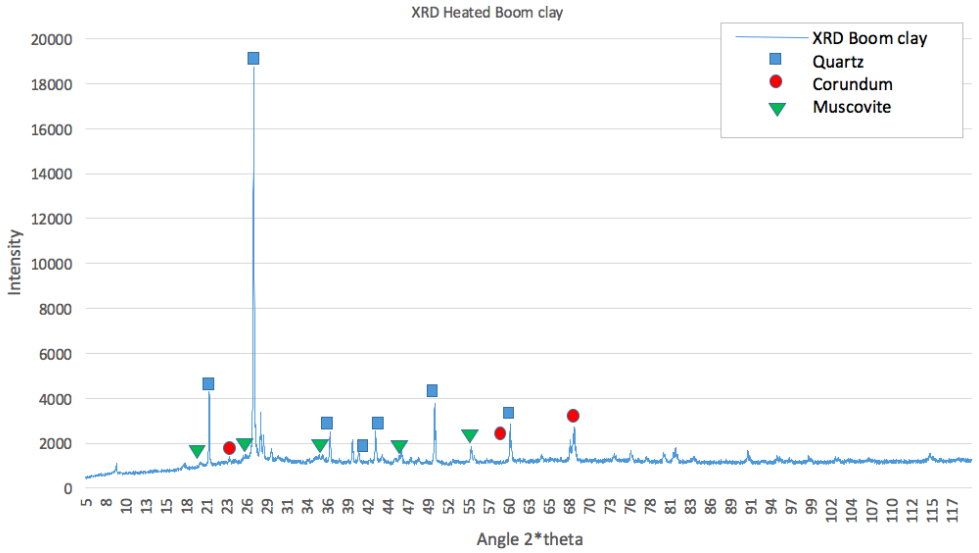

FIGURE 4.11: Diffractogram of the heated Boom clay and the three main phases, quartz, corundum and muscovite.

4.2.5 Discussion

The Positron Doppler Broadening experiment is plotted with the TG (figure 4.12) and DSC (figure 4.13) curves respectively.

The first thing that stands out is the peak of the S parameter from 170°C to 350°C. The dissipation of water and structural water occurs from 50-350°C, so this peak is probably caused by the creation of vacancies because of the water loss. Between 350°C and 480°C the S parameter drops to values lower than the room temperature values. This indicates the vacancies that were present at 350°C have changed. Figure 5.9 shows this drops occurs at the same temperature as the drop assigned to the oxidation of pyrite. In figure 5.10 you can see the S parameter falls at the same time as the heatflow curve, this drop in heatflow was assigned to the oxidation of pyrite. It is possible the vacancies disappear due to some phase transition that changes the molecular structure.

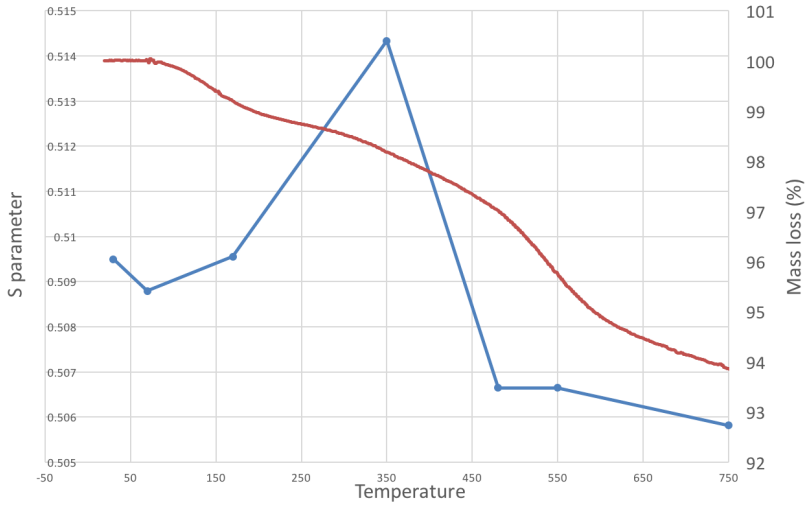

FIGURE 4.12: S-parameter and mass loss (%) vs temperature

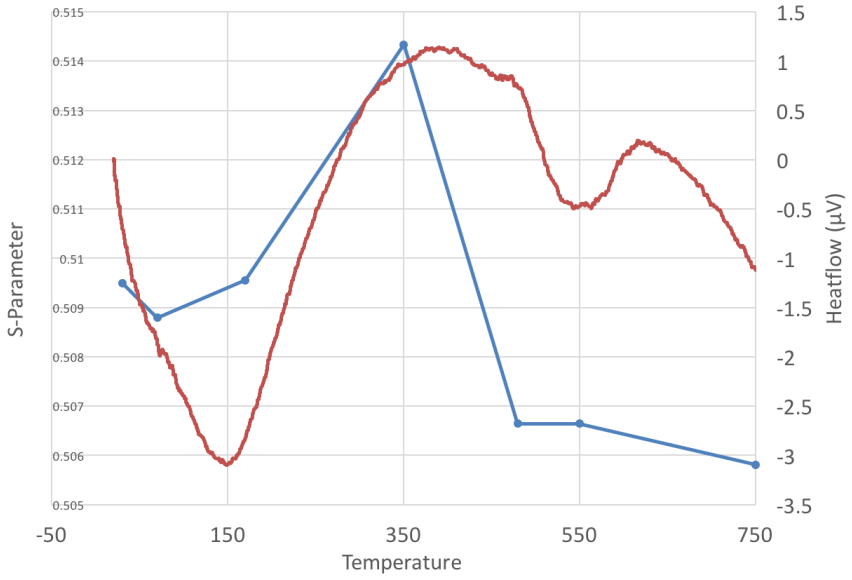

FIGURE 4.13: S-parameter and heatflow (μV) vs temperature

Because the only PALS measurements were done at room temperature and at 750°C, it is hard to draw conclusions from the lifetime experiment. However there is some interesting information in it. The PALS showed a somewhat shorter lifetime for the heated sample which is consistent with the Doppler Broadening experiment. The PALS measurements also showed a longer lifetime which suggest the formation of positronium in a larger open volume.

Chapter 5

Conclusions

The study on NZP phosphates clearly showed the correlation between the vacancies density in $Sr_{1-(x/2)}[Zr_{1+x}Fe_{1-x}(PO_4)_3]$ and the S parameter of the DBAR experiment. A higher vacancy density resulted in a higher S parameter which indicates a higher porosity. It was also shown with XRD that this correlation was not caused by changes in the dimensions of the unit cell. So it can be concluded positrons annihilation is a powerful tool to study defects and vacancies in materials.

The DSC-TG experiment on the Dutch Boom clay indicates multiple phase changes and mass losses with temperature. The (structural)water loss at temperatures around 50-350 was seen as an increase of the S parameter which indicates a higher porosity. Higher temperatures showed a decrease in the S parameter which indicates a lower porosity. This could be caused by a phase change of a mineral inside the clay that changes the molecular structure. But more intensive mineralogical studies have to be done to conclude where this effect comes from. The PALS measurement showed a somewhat shorter lifetime in the heated sample which agrees with DBAR. To draw more conclusions from PALS, measurements have to be done at different temperatures.

Appendix A

Acknowledgements

I would like to thank Denis Bykov for the supervision and guidance along this research. Furthermore I would like to thank Andrea Sabau for all the help concerning the Boom clay part of this thesis and Henk schut for the teaching and assistance with the positron measurements. I would also like to thank Maarten Plokker and Maik Butterling for helping me with the VEP and interpretation of the data.

Appendix B

Future work

B.0.1 NZP Phosphates

If in future work it is possible to determine the atomic positions with XRD, the value of the S parameter can be compared with the sizes of the vacancies. This gives insight into the DBAR technique. Also a PALS measurement can be done on all the samples to investigate the sizes of the vacancies.

B.0.2 Boom clay

In future work more PALS measurements can be done in the temperature range 150-450°C to see when the large peak occurs precisely, to check what caused this peak a more extensive mineralogical research has to be done on the clay.

Bibliography

[1] R.B. Wiegers E.A.C. Neeft G. Deissmann E.V. Verhoef, A.M.G. de Bruin. Cementitious materials in opera disposal concept in boom clay. *Opera*, page 3, April 2014. URL http://www.covra.nl/downloads/opera.

[2] http://www.cebama.eu/. 2015.

[3] L.M. van Koppen. Nzp-type ceramics for simultaneous incorporation of radioisotopes of cesium strontium and minor actinides. *Bachelor Thesis*, page 3.

[4] J.-M. Montel. Minerals and design of new waste forms for conditioning nuclear waste. *Comptes Rendus Geoscience 343*, page 230, 2011.

[5] J-L. Kloosterman Denis Bykov, R.J.M. Konings. Nzp phosphates as alternative waste forms for the separated waste fractions. *Section Nuclear Energy and Radiation Applications Department of Radiation Science and Technology.*

[6] K.A. Thomas B. Sivasankar G.V. Subba Rao, U.V. Varadaraju. Metal atom incorporation studies on the phases with nzp structure: Nbtip3o12. *Journal of solid state chemistry*, 1987.

[7] Alex P. Meshik. The workings of an ancient nuclear reactor. *Scientific American*, January 2009. URL https://www.scientificamerican.com/article/ancient-nuclear-reactor/.

[8] J.Griffioen M. Koenen. Mineralogical and geochemical characterization of the boom clay in the netherlands. *Opera*, page 3, November 2014. URL http://www.covra.nl/downloads/opera.

[9] Haofeng Xing Yuliang Zhang Hui Sun Jie Han, Qiang Sun. Experimental study on the thermophysical properties of clay after high temperatures. *Elsevier*, july 2016.

[10] W. Bastiaens J. Verstricht G. Chen J. Leysen J. Rypens Ph. van Marcke, X.L. Li. The design and installation of the praclay in-situ experiment. *EURIDICE REPORT*, (13-129), 2013.

[11] T. Oka K. Hirata Y. Kobayashi, K. Ito. Positronium chemistry in porous materials. *Elsevier*, pages 224–230, 2007.

[12] z y Joseph H. Hadley Jr. z Frank H. Hsu z Eric R. Vance, w and Elizabeth Drabareky. Positron annihilation lifetime spectra in a metakaolin-based geopolymer. *The American Ceramic Society*, 191, 2007.

[13] K Sudarshan J David J F Williams C Ranganathaiah P Guagliardo, E R Vance and S Samarin. Positron annihilation study of cs-deficient pollucite.

[14] K. Orzechowskia K. Jerieb A. Baranowskib T. Slonkac K. Leluka, and J. Glowinski . Positron annihilation lifetime spectroscopy and dielectric measurements of natural kaolinite and kaolinite intercalated by potassium acetate.

[15] L.-O. Hagman and P. Kierkegaard. The crystal structure of name (po) ; me=ge, ti, zr. *Acta chemica scandinavica*, 1968.

[16] K. Momma and F. Izumi. "vesta 3 for three-dimensional visualization of crystal, volumetric and morphology data,". *Crystal Impact*, pages 1272–1276, 2011.

[17] Rao G.V.S. Sugantha M., Varadaraju U.V. J. solid state chem. (111):33–40, 1994.

[18] Shrivastava Rashimi C. Solid state sci. (13):444–454, 2011.

[19] Dr. Holger Putz. Dr. Klaus Brandenburg. Pearson's crystal data. *J. Appl. Crystallogr., 44*, pages 1272–1276, 2016. URL http://www.crystalimpact.com.

[20] J.-Y. (ed.) Boisson. Ea rapport 4436. *Clay Club Catalogue of Characteristics of Argillaceous Rocks*, (92-64-01067-X):27/72, 2005.

[21] Commissie Opberging Radioactief Afval. Terugneembare berging een begaanbaar pad, februari 2001. *Ministerie van Economische Zaken*, page 24/110, 2001.

[22] Ebbing JHJ De Lang FD. Beschrijving van de lithografische eenheid: Rupel formatie. *TNO-NITG*, pages 1–6, March 2003.

[23] Timescale and age according to tectono-stratigraphic charts of the netherlands continental shelf. *TNO publication*, pages 1–8, February 2011.

[24] Arjen Poley (NRG) Ewoud Verhoef, Erika Neeft (COVRA N.V.) Jacques Grupa. Outline of a disposal concept in clay. *Opera*, page 3, November 2014. URL http://www.covra.nl/downloads/opera.

[25] J. Griffioen M. Koenen. Mineralogical and geochemical characterization of the boom clay in the netherlands. *Opera-PG-COV008*, November 2014.

[26] A.M.Tang P. Delage, Y.J.Cui. Clays in radioactive waste disposal. *Journal of rock mechanics and geotechnical engineering*, November 2009.

[27] Michael A. Hicks Jan Fokkens Patrick Arnold, Philip J. Vardon and Peter A. Fokker. A numerical and reliability-based investigation into the technical feasibility of a dutch radioactive waste repository in boom clay. *Opera-PU-TUD311*, Januari 2015.

[28] Andrea Sabau. Xrd dutch boom clay. *RID*, 2016.

[29] Hartmut S. Leipner Reinhard Krause-Rehberg. Positron annihilation in semiconductors. 2010.

[30] Iri Escobar. Chapter 2 thesis iri escobar: Basic concepts: Experimental techniques and positron modelling. 10 2002.

[31] J. Kansy. Lt. *Nucl.InstrMeth A374*, (23), 1996.

[32] J.L. Powell A. Ore. *Phys. Rev.*, 82(23):455, 1949.

[33] E.M. Lifshitz V.B. Beretetskii. Relativistic quantum theory. *Pergamon Press*, (23), 1971.

[34] M.A. Pedrosa Luna. Aplicacuib de ka technica de aniquilacion de positrones al estudio de oxidos cristalinos y amorfos. *Phd Thesis*, (23), 1988.

[35] Christine M. Clark Eastern Michigan University Barbara L Dutrow, Louisiana State University. X-ray powder diffraction (xrd). *Geochemical Instrumentation and Analysis*. URL http://serc.carleton.edu/research_education/geochemsheets/techniques/XRD.html.

[36] Gregors; https://commons.wikimedia.org/wiki/User:Gregors. X-ray diffraction. *derivative work on wikipedia*. URL https://en.wikipedia.org/wiki/Bragg27s_law.

[37] Confederation of national or regional thermal analysis and calorimetry societies. URL http://www.ictac.org/index.html.

[38] David Dollimore. Thermal analysis. (10.1002/0471266965.com027):337–390, October 2002.

[39] Makhov A.F. *Sov. Phys. Sol. State*, (2), 1934.

[40] P. Hautojarvi A. Vehanen, K. Saarinen and H. Huomo. Profiling multilayer structures with monoenergetic positrons. *Physical review 8*, 35(10), April 1987.

[41] Setaram instrumentation. URL http://www.setaram.com/.

[42] H.; Clement M.; de Nijs J. M. M.; Kruseman A.; IJpma M. R. van Veen, A.; Schut. Vepfit applied to depth profiling problems. *Applied Surface Science*, 85:216–224, January 1995.

[43] J. Rodriguez-Carvajal. Physica b. (192):55, 1993.

[44] A LeBail. Whole powder pattern decomposition methods and applications: A retrospection. *Powder Diffraction*, 20, 205.

[45] M. Azmi Bustam T. Murugesan Ali. E. I. Elkhalifah, Saikat Maitra. Thermogravimetric analysis of different molar mass ammonium cations intercalated different cationic forms of montmorillonite. *J Therm Anal Calorim*, July 2011.

[46] J. Ladrire F. Dussart J. Dabi O. Haulotte S. Verhaeghe J. Regout. Mssbauer study of the boom clay, a geological formation for the storage of radioactive wastes in belgium. *Hyperfine Interactions*, 191, 2009.

[47] S.Dhanapandian R.Venkatachalapathy C.Manoharan, P.Sutharsan. Characteristics of some clay materials from tamilnadu india, and their possible ceramic uses. *Ceramica*, 58, 2012.

[48] Panalytical xray diffraction software. *http://www.panalytical.com/Xray-diffraction-software/HighScore/Specifications.htm*.